The emergence of multifrequency force microscopy

Ricardo Garcia* and Elena T. Herruzo
IMM-Instituto de Microelectrónica de Madrid, CSIC, Isaac Newton 8, 28760 Tres Cantos, Madrid, Spain.

*e-mail:ricardo.garcia@imm.cnm.csic.es

Atomic force microscopy uses the deflection of a cantilever with a sharp tip to examine surfaces, and conventional dynamic force microscopy involves the excitation and detection of a single frequency component of the tip's motion. Information about the properties of a sample is, however, encoded in the motion of the probe and the dynamics of the cantilever are highly nonlinear. Therefore, information included in the other frequency components is irreversibly lost. Multifrequency force microscopy involves the excitation and/or detection of several frequencies of the probe's oscillation, and has the potential to overcome limitations in spatial resolution and acquisition times of conventional force microscopes. It could also provide new applications in fields such as energy storage and nanomedicine. Here we review the development of multifrequency force microscopy methods, highlighting the five most prominent approaches. We also examine the range of applications offered by the technique, which include mapping the flexibility of proteins, imaging the mechanical vibrations of carbon-based resonators, mapping ion diffusion, and imaging the subsurface of cells.

The atomic force microscope (AFM) has been a key instrument in the development of nanoscience and nanotechnology over the last 25 years[1]. It measures the static deflection of a probe (cantilever-tip system) while the probe is displaced across the surface of a sample, and in its original mode (contact AFM) the tip is always in mechanical contact with the surface. The development of the AFM was a significant conceptual breakthrough with respect to existing microscopes, which used either electrons or photons as imaging agents. However, the first images, taken of a ceramic surface (Al_2O_3), barely hinted the existence of nanoscale spatial resolution[1]. Since then the instrument has undergone several notable technical advances, including the development of a robust, reliable and sensitive detection scheme (the optical beam deflection method)[2]. This method paved the way for the manufacturing of commercial instruments.

Another important development has been the implementation of dynamic AFM methods[3-4]. These methods involve the excitation of the probe at a single frequency, while the probe is displaced across the sample surface. A feedback loop keeps one of the parameters of the oscillation, either the amplitude or the frequency shift, at a fixed value. The oscillation parameters depend on the tip-surface separation, consequently

atomic or nanoscale changes in the topography will imply changes in the distance and, those in turns, in the probe's oscillation parameters. By compensating those changes, the feedback loop generates high resolution images of the surface topography. Dynamic AFM methods have four major advantages with respect to contact AFM. (1) It is easier to image at small forces (such as in the 1nN range) especially in air. This, in turn, allows soft materials to be imaged. (2) Lateral forces are suppressed. (3) Observables such as the amplitude, the phase, the frequency or the cantilever deflection are available and can be used to extract information on the properties of a material. (4) Atomic resolution imaging of reactive surfaces in ultrahigh vacuum can be achieved due to control over the mechanical contact between the tip and the surface atoms.

The reduction of the force exerted by the tip on the sample has been essential in allowing a variety of soft materials, such as DNA, proteins, cells or polymers[5-8], to be studied with relative ease. The reduction of the force has also lead to atomic and molecular resolution images in a variety of environments[9-14]. Furthermore, dynamic AFM provided a suitable experimental set-up to combine topography with the mapping of electrostatic[15] or magnetic[16] properties.

The impact of force microscopy also goes beyond the field of high resolution imaging: AFM has lead to a renaissance in mechanics, or more accurately, nanomechanics. Nanomechanics provides the basis to explain the operation and the performance of the AFM[3,17-19]. Moreover, mechanical forces play fundamental roles in biology and the AFM can be used to precisely measure the binding forces between individual biomolecules or the local stiffness of biomaterials (force spectroscopy)[20-21]. For example, force spectroscopy has been used to study the nanomechanical properties of cells[22], which could be relevant to analysing the progression of tumours[23]. In addition, AFM technology has lead to the development of very sensitive micro and nanomechanical devices[24-25].

The prominence of AFM has also raised expectations in terms of spatial resolution, quantitative measurements and data acquisition times, but the technique currently faces a number of limitations. In fact the proven strengths of the technique illustrate some of these limitations. Atomic and molecular resolution imaging in air, liquid or ultrahigh vacuum is arguably the most striking feature of the instrument. However, high resolution imaging is a property that depends as much on the mechanical properties of the material under study, as it does on the sensitivity and resolution of the microscope. Molecular resolution images are either hard to obtain or, in the case of very soft materials such as those with an effective elastic modulus below 10 MPa (isolated proteins, cells, some polymers), have not been obtained. Similarly, it is hard to combine the exquisite force sensitivity of force spectroscopy with molecular resolution imaging, and simultaneous high spatial resolution and material properties mapping is therefore challenging.

The conventional AFM is a surface characterization technique, and the non-invasive imaging of buried structures (subsurface imaging) is not considered a mainstream activity. Similarly, processes, such as subsurface ion diffusion in batteries, have been beyond the realm of the AFM either because of a lack of sensitivity or because of difficulties in separating elastic from non-conservative components in the measured force.

To expand the capabilities of the AFM and to overcome its current limitations two principles need to be considered: (1) all the information about the properties of a sample are encoded in the probe's motion; and (2) the dynamics of the microcantilever are highly nonlinear and therefore the harmonics and lower eigenmodes components are integral parts of the tip's motion. Conventional dynamic AFM methods involve the excitation and detection of a single frequency component of the tip's motion. Therefore, the information about the properties of a sample that is included in the other frequency components is irreversibly lost.

Multifrequency AFM methods involve the excitation and/or detection of several frequencies of the probe's oscillation. Those frequencies are usually associated with either the higher harmonics of the oscillation or the eigenmodes of the microcantilever. Multifrequency excitation/detection schemes provide higher sensitivity and resolution because these methods are specifically designed to decode the information generated by the nonlinear regions of the tip-surface interaction force.

The physics of multifrequency AFM methods

There are two main dynamic AFM methods: amplitude modulation AFM (AM-AFM) and frequency modulation AFM (FM-AFM)[3,4,26]. In AM-AFM, the probe is excited at a fixed frequency and the amplitude is held constant by the feedback loop while taking an image. In FM-AFM the frequency shift is held constant by the feedback loop. A single frequency is used for the excitation and detection of the cantilever motion. This frequency is commonly tuned (or is very close) to the 1st resonance (eigenmode). The purpose of any dynamic AFM experiment is to recover the information about the sample's properties encoded in the microcantilever dynamics.

The cantilever dynamics are nonlinear[3,18-19,26] because the amplitude of the oscillation is higher than the decay lengths of the interaction forces. For atomic and molecular resolution images the decay lengths are about 0.5 nm, while the amplitudes are in the 1-10 nm range. To be precise, the nonlinear effects relevant for high resolution imaging and mapping of material properties are examples of mild nonlinear dynamics. In some situations, the microcantilever could experience very complex trajectories[18-19]. However, the presence of extreme nonlinear behaviour in force microscopy can be easily avoided by a proper selection of the operational parameters.

The presence of several frequency components in the tip's oscillation has been known for several years[27-32]. However, the role of those components on the spatial resolution, time-dependent process and material properties sensitivity has been either overlooked or neglected due to at least three factors. First, those components were observed by applying large tip-surface forces, which are not suitable for high resolution imaging[32]. Second, in typical experimental conditions, the higher harmonics components are several orders smaller than the fundamental frequency component[32-33]. To observe them requires either improving the signal-to-noise ratio of the instrument or developing specific experimental methodologies to enhance them. Finally, a comprehensive theory to decode the information about the sample properties in terms of the frequency components is complex and was not initially in place.

The microcantilever probe is a mechanical system and as such it is characterized by its eigenmodes and their respective properties[33-45]. The eigenmodes are also called normal modes or resonances. They are characterized by four parameters, the effective stiffness k_i (force constant), the resonant frequency $\omega_i=2\pi f_i$, the quality factor Q_i and the optical sensitivity σ_i. For a rectangular and tipless microcantilever there are several relationships among the above parameters (Table 1). The above relationships are approximations to describe real AFM microcantilevers. The tip mass, the presence of a picket at the end of the cantilever or a non-uniform cantilever's cross-section along its length could introduce significant changes in the mode shape[38,45,51] that would limit the validity of the analytical expressions.

The nonlinearities in the interaction force introduce higher harmonics components in the probe's motion. Thus, the tip-surface force is encoded in the frequency spectra of the tip motion. The harmonics vibrate with a frequency equal with an integer multiple of the excitation frequency ($n\omega$) (Box 1). The amplitude of the higher harmonics is proportional to the convolution of the force over the harmonic wave form[46] (Box 2). The theoretical analysis also shows that the amplitude of the higher harmonics decreases with the order as $\sim 1/n^2$. When the oscillation amplitude is comparable to the range of the short-range forces, the higher harmonics are proportional to the higher force gradients[47-48].

The higher harmonics act as effective driving forces that excite the vibration of the higher eigenmodes of the cantilever. This happens whenever the frequency of a higher harmonic is close to that of an eigenmode[33,35]. For a rectangular and tipless microcantilever, the frequency of the 2nd eigenmode is $6.27\omega_0$, this is very close to that of the 6th harmonics ($6\omega_0$). As a consequence, the frequency spectra are modulated by the presence of the eigenmodes (Fig. 1e). The above description is supported by both numerical simulations and experimental observations. In liquid, the momentary excitation of the 2nd eigenmode plays a relevant role in the cantilever dynamics[49].

The presence of higher harmonics in the deflection signal allows time-resolved forces to be obtained and thus to measure the sample dynamics in a time frame of

microseconds. This method can be divided in two steps[50]. The first step requires the cantilever trajectory to be expressed in the frequency domain. The second step implies to perform the inverse Fourier of the cantilever trajectory divided by its transfer function. However, it requires a relatively large number of harmonics (~15) to get accurate estimations of the force. Special cantilevers are required to enhance the number of higher harmonics in the probe's oscillation[51-53]. In particular, the torsional harmonic cantilevers has improved the signal-to-noise ratio of the higher harmonics and simplified the calculation of the transfer function[54].

The multifrequency aspects of dynamic AFM have been overlooked because the high frequency components are usually very small. For example, it has been shown that for high *Q* cantilevers (Q≥50), the amplitudes of the higher harmonics are two-to-three orders of magnitude smaller than the fundamental component[33]. The amplitude of the higher eigenmodes can be enhanced by exciting simultaneously several of them, the simplest case being the excitation of the first two eigenmodes[55-57]. By recording the signal at the excited frequencies different channels, one per excited eigenmode, are available to acquire complementary information on the sample properties[58-61]. This approach has several advantages. For example, in AM-AFM the feedback imposes considerable restrictions on the information conveyed by the phase shift of the mode used by the feedback frequency. Those restrictions do not apply to the information carried by the 2nd excited eigenmode[60]. In addition, the simultaneous excitation of two modes also enhances the coupling of those modes by the nonlinear force. This also contributes to increase the sensitivity of the 2nd mode to detect material properties[56]. It has also been shown that for small amplitudes, the parameters of the 2nd mode can be related to the force gradient[58,61], which also explains the higher sensitivity of bimodal AFM to detect variations in material properties.

This approach has been extended to the simultaneous excitation of three eigenmodes[62] and to non-resonant frequencies, for example, to two frequencies that are in the vicinity of a resonance[63-64]. The tip-surface forces generate a new set of frequencies called intermodulation products[63] which also encode the interaction force. There are other remarkable results brought by the simultaneous excitation of several frequencies near the fundamental resonance such as the real time determination of the effective cantilever parameters[65-66] or the control of some nonlinear dynamics properties[67-68].

The use of higher flexural eigenmodes for imaging (single excitation/detection) has been suggested to avoid the jump-to-contact phenomenum[69-71]. However, the higher the eigenmode the lower the sensitivity to the properties of a material. The sensitivity of a mode depends on the Q_i/k_i ratio[72] which, for an ideal cantilever, decreases with the eigenmode order (Table 1).

Multifrequency AFM methods

There are several multifrequency AFM methods. However, five of them currently provide the majority of experimental applications (Fig. 2).

Multi-harmonics AFM imaging. This is the most straightforward approach to perform a multifrequency AFM experiment. It requires just the recording and subsequent plotting of the higher harmonics components generated while acquiring a topography image in conventional dynamic AFM modes[73-80]. However, the detection of higher harmonics in air is hard to achieve under the application of the forces required for high resolution imaging[6,8] (sub-1 nN, for example). For this reason the use of special cantilevers that allowed the tuning of a higher eigenmode with a higher harmonic has been suggested[51]. The fact that in liquid the higher harmonics are easier to detect has allowed the imaging of a bacterial S-layer with 0.5 nm spatial resolution by plotting the amplitude of the 2nd harmonic of the fundamental frequency[78]. The same method has been applied to image a living bacteria[79] with an enhancement in contrast. The combination of several harmonics, in particular, the zeroth, first and second harmonics has allowed the nanoscale mapping of the local stiffness and viscolelastic dissipation in living cells[80]. In ultrahigh vacuum, the use of higher harmonics has revealed features with a lateral distance of only 77 pm on a tungsten surface[47].

Bimodal AFM. This method uses two driving forces to excite the vibration of the microcantilever[55-58,81](Fig. 2b). The excitation frequencies are tuned to match two of the flexural eigenmodes of the cantilever, usually the first and the second eigenmodes. An output signal of the first mode (either the amplitude or the frequency shift) is used to image the topography of the surface while the output signals of the second mode (amplitude and/or phase shift) are used to measure changes in mechanical[81-85], magnetic[72,86] or electrical properties[87-88] of the surface. This method is compatible with both dynamic AFM modes and can be performed in air[81], liquid[56-57] an ultrahigh vacuum[58,89]. Bimodal AFM has been operated at very low forces (50 pN) in liquid which has enabled the non-invasive imaging of isolated proteins[61].

Bimodal AFM offers a straightforward approach to separate topography from other interactions influencing the tip motion such as magnetic or electrostatic forces. Thus, the different resonances of the cantilever could be seen as channels to access and separate different sample properties. To avoid the excitation of non-periodic oscillations some restrictions on the values of the amplitude ratio between the excited resonances must be implemented[56,84].

Band excitation. This method introduces a synthesized digital signal that spans a continuous band of frequencies, and monitors the response within the same or even larger frequency band[65,90-91]. The method aims to improve the ability to acquire different dynamic curves while the topography of the surface is recorded. The cantilever response is detected using high speed data acquisition methods and then Fourier transformed. The resulting amplitude-frequency and phase-frequency curves are collected at each point of the surface and stored in three dimensional data arrays. This

data is analyzed to extract some of the relevant parameters that characterize the cantilever behaviour (Fig. 2c). For example, in the single harmonic oscillator approximation, the resonant frequencies, the amplitude and the *Q* are deconvoluted and stored as images. Furthermore, in the case of adaptive control it can be used as a feedback signal in microscope operation.

Band excitation has been applied to probe the electromechanical coupling in soft biological systems by distinguishing among damping, Young modulus and electromechanical contributions. Notably, it has also been used to study ion diffusion in electrochemical batteries[90-91]. However, the large amount of data generated in a band excitation experiment together with the need for sophisticated controllers might become major obstacles for a wide use of this approach.

Torsional harmonic AFM. This is an approach based on the recording of the higher harmonics of the torsional signal[54,92-93]. Torsional harmonic can be used to generate a topographic image of the sample surface at the same time that the time-varying forces are recorded. The topographic image is a conventional AM-AFM image. At the same time, the tip-surface force is obtained by integrating the higher harmonics of the torsional signal. Torsional harmonic AFM requires the use of specially designed cantilevers where the tip is offset from the cantilever axis (Fig. 2d). This design favours the existence of a torque around the axis of the cantilever which enhances the presence of the large number of higher harmonics needed to have an accurate calculation of the time-varying force[92]. From those forces is possible to measure locally some mechanical properties, such as the Young modulus[93]. Remarkably, those measurements have been also applied to detect and quantify DNA molecules[94] and to measure molecular recognition processes[95]. Torsional harmonics AFM measurements have revealed significant differences in the fractal dimensionality of cancerous cells with respect to normal cells[96]. These measurements underline the potential of multifrequency AFM in nanomedicine.

Nanomechanical holography. This technique combines elements derived from ultrasonic[97-98]and dynamic force microscopies[3] to generate images of structures that lie below the surface of biological or synthetic materials[99-100]. It is based on the simultaneous excitation of the sample and the probe[99-103]. The mechanical excitation of the sample generates waves that propagate through the sample. Those waves are scattered by the internal features or structures of the material. As a consequence, the amplitude and the phase shift of the waves are modified by the interaction with the inner structures of the material. The modification depends on the local mechanical properties of the features. Eventually the scattered waves emerge on the surface where they influence the tip-surface coupling.

In some cases the coupling of the sample and tip's vibrations generate a new set of frequencies that are a linear combination of the frequencies used to excite the tip and the sample, the simplest case being the difference between them. An image of the

subsurface structure is acquired by plotting the phase shift of one of the synthesized modes as the probe moves across the sample surface. Nanomechanical holography has been applied to image the inner structure of different cells[99-100], and in particular, the presence of nanoparticles inside soft materials[101] or in the lung cells of mice exposed to single-walled carbon nanohorns[102]. It is also applied to investigate the dimensionality and fatigue performance of buried of electrical contacts and interconnects in microelectronics devices[103]. However, difficulties in interpreting the images in terms of the properties of the sub-surface structures pose challenges for the progress of the technique.

Applications

The flexibility, sensitivity and potential of multifrequency AFM methods are illustrated by their applications in different fields, which range from energy storage to nanomedicine. In these areas the multifrequency methodologies are being applied to investigate properties that are not easily accessible by conventional AFM methods.

Mapping protein flexibility with molecular resolution. Protein flexibility plays a central role in the binding to other proteins either isolated or embedded in a membrane as cell receptors. Current methods for the determination of the protein flexibility give results in a time scale of picoseconds that might not be relevant to the conditions where proteins have conformational changes in physiological conditions (micro- to milliseconds). Multifrequency AFM methods have measured with molecular resolution the flexibility of several proteins in liquid (Fig. 3). Torsional harmonic AFM has mapped the flexibility of proteins in purple membrane sheets at the microsecond time scale by monitoring surface-induced deformations[93] (Fig. 3a-c). The measurements show differences in the flexibility between the cytoplasmatic (4-10 MPa) and extracellular sides (15-50 MPa) of the membrane.

Complementary experiments have been performed with a bimodal AFM by mapping the topography and the flexibility of isolated proteins in physiological conditions[61] (Fig. 3d-f). The images of single proteins (antibodies) have been obtained noninvasively because the bimodal approach in combination with FM-AFM enables imaging under the application of very small forces (below 50 pN). Figure 3d shows the topography of a single protein complex and Fig. 3e the corresponding flexibility map (local variations of the elastic modulus) (see Box 3). The flexibility map shows a maximum of 19 MPa and a minimum value of 8.2 MPa. The comparison between the flexibility map and the structure of the protein complex shows that the uppermost part is stiffer as a consequence of the presence of intermolecular disulfide bonds joining different fragments of the protein complex. On the other hand, low elastic modulus values are found in the last domain of the antigen binding arms. The above findings are consistent with the orientation flexibility of the antibody complex when its binds a cell surface antigen.

Imaging the mechanical vibrations of carbon-based resonators. Carbon nanotubes and graphene sheets have been used to fabricate mechanical resonators that can be operated at ultrahigh frequencies, have tunable resonance frequencies, and can be used as ultrasensitive inertial mass sensors[24-25,104]. A variation of the bimodal AFM approach has been implemented to detect, identify and image the spatial shape of the eigenmodes of these resonators[104-105](Fig. 4a,b). This method has enabled the observation of a new class of exotic nanoscale vibration eigenmodes not predicted by the elastic beam theory, where the amplitude of vibration is maximum at the free edges[105]. The motion of the suspended resonators was electrostatically driven by applying a voltage (V_{RF}). Because the resonances of nanoscale resonators are far above the mechanical response of AFM microcantilevers, the excitation voltage of the resonators was modulated at the frequency of the 1st eigenmode of the cantilever (Fig. 4a). The mechanical vibrations were detected and imaged by following the changes of the envelope of the vibration amplitude. Figure 4b shows an AFM image of a suspended carbon nanotube and its first three eigenemodes.

Mapping ion diffusion. Lithium-ion batteries are common in applications such as mobile electronic devices and electric and hybrid vehicles. The movement of lithium ions into and out of electrodes is central to the operation of those batteries. However, this displacement has not been described at the nanoscale which, in turns, limits the understanding of the mechanisms underpinning lithium-ion battery operation. Band excitation experiments have demonstrated the existence of a strong coupling between lithium ion concentration and cathode lattice parameters[90-91]. Those experiments have established that the diffusion coefficient increases for certain grain orientations and single-grain boundaries (red regions in Fig. 4e). The lateral resolution ~20 nm allows Li-ion motion to be probed in 10^6 smaller volumes than possible by classical current-based electrochemical methods. These results offer a direct path to improving the electrochemical performance of Li-ion batteries. In the above measurements the sensitivity of the band excitation method enabled measuring the changes in the lattice parameter associated with the ion diffusion and migration.

Subsurface imaging in cells. Imaging structures beneath the surface of a sample with sub-100 nm spatial resolution has always been a formidable challenge in microscopy. Typically, high-resolution images of a subsurface structure are obtained by slicing the material and observing the newly created surface. However, this approach damages the sample under study. Nanomechanical holography has demonstrated its potential for the non-destructive imaging of embedded or buried substructures of several animal and plant cells[99-100]. Remarkably those experiments have been performed without any labels or sectioning of cells, and under physiologically viable conditions. Figure 4g shows a nanomechanical holography image taken simultaneously with a conventional AFM image (Fig. 4h). Several features of the cell substructure such as the cell walls and the nucleus are resolved in the image. In comparison, the conventional AFM image shows a featureless object.

Summary and outlook

Force microscopy is evolving from single excitation and detection schemes to multifrequency excitation and detection schemes. This development is being driven by a variety of reasons. There is, for example, a need to operate the instrument under very low forces. Alternatively, there is a need to improve the spatial resolution of soft materials or to measure quantitatively surface properties without compromising fast data acquisition times. There is also a need to find new applications in fields such as materials science or nanomedicine.

Multifrequency AFM can be classified as a new field in force microscopy due to the diversity of multifrequency approaches available, the use of novel excitation or detection schemes, and the emphasis placed on mixing several frequencies. This field provides a promising framework to improve compositional sensitivity, spatial and time resolution of materials in their native environment and, at the same time, allows properties that are not accessible to conventional force microscopes to be measured. Multifrequency AFM methods are conceptually more demanding than conventional AFM methods, but this would appear to be a reasonable price to be pay in order to sustain the impressive development of force microscopy that has been seen over the last 25 years.

Acknowledgement. We thank the financial support from the Ministerio de Ciencia e Innovación (CSD2010-00024, MAT2009-08650).

Box 1: Approximations for the microcantilever deflection

Different degrees of accuracy and complexity can be applied to describe the steady-state deflection of the microcantilever. The most common assumption is to consider a sinusoidal solution,

$$z = z_0 + A\cos(\omega t - \phi) \qquad (1)$$

where A, z_0 and φ are, respectively, the amplitude, the static component of the deflection and the phase shift with respect to the driving force. Equation 1 neglects any multifrequency components. The next approximation level considers the presence of high frequency components (harmonics). The harmonics are naturally generated when the vibrating probe is exposed to the nonlinear regions of the interaction force, then

$$z = z_0 + \sum_{n=1}^{N} A_n \cos(n\omega t - \phi_n) \qquad (2)$$

where A_n is the amplitude of the harmonic with angular frequency $n\omega$. Equations (1-2) are compatible with a point-mass description of the microcantilever.

A more precise description is achieved by considering the extended character of the cantilever. Then, the probe's deflection contains contributions from all its eigenmodes (q_j),

$$z = z_0 + \sum_{j=1}^{M} q_j(t) = z_0 + \sum_{n=1}^{N} A_n \cos(n\omega t - \phi_n) \qquad (3)$$

In Eq. (3) the eigenmodes have been expressed in terms of the different harmonics (A_n) .

Box 2: The interaction force and the harmonics

The harmonics and the forces are related by an integral expression. This relationship is obtained by multiplying the Equation of motion by $\cos(n\omega t - \phi_n)$ and $\sin(n\omega t - \phi_n)$ and integrating over a period. In amplitude modulation AFM, the higher harmonics can be expressed as

$$A_n = S\frac{\omega_0}{k}\sqrt{\left(\int_0^T F_{ts}(d)\cos(n\omega t)dt\right)^2 + \left(\int_0^T F_{ts}(d)\sin(n\omega t)dt\right)^2} \qquad (4)$$

$$S \approx \frac{1}{\pi n^2} \quad \text{and} \quad n>3 \qquad (5)$$

where d is the instantaneous tip-surface distance. For oscillations where the repulsive region of the interaction potential is stronger than the attractive region, the higher harmonics components can be parameterized in terms of the maximum force (F_{max}) and the contact time t_c,

$$A_n = A_n(F_{\max}, t_c, n) \qquad (6)$$

In frequency modulation AFM, the higher harmonics can be expressed in terms of the force by

$$A_n = \frac{2}{\pi k}\frac{1}{1-n^2}\int_{-1}^{1} F_{ts}^{n}(z_c + z_0 + A_1 u)\frac{T_n(u)}{\sqrt{1-u^2}}du \quad (7)$$

where $T_n(u)$ is the n-th Chebyshev polynomial of the first kind, z_c the average position of the cantilever and $u = \cos\omega t$.

Box 3: Simultaneous topography and flexibility mapping

In bimodal AFM the tip's motion can be approximated as

$$z = z_0 + q_1(t) + q_2(t) = z_0 + A_1\cos(\omega_1 t - \phi_1) + A_2\cos(\omega_2 t - \phi_2) \quad (8)$$

where A_i, φ_i are the amplitudes and phase shifts of the excited modes. The application of the virial theorem to the free eigenmode (the second) in bimodal AFM gives a relationship between the parameters of the second mode and the gradient of the interaction force. Then, by applying contact mechanics the sample flexibility can be obtained in terms of the amplitude and phase shift of the 2nd mode. From the virial theorem it is deduced ($A_{02} << A_{01}$)

$$\frac{dF_{ts}}{dz}(d) \approx C\frac{k_2 A_{02}}{Q_2 A_2}\cos\varphi_2 \quad (9)$$

where A_{02}, k_2, ω_2 and Q_2 are, respectively, the free amplitude, force constant, angular resonant frequency and quality factor of the 2nd eigenmode. C is a correction factor that converges to a constant value for high A_{01}/A_{02} ratios. Finally, by applying the Hertz contact mechanics model,

$$\frac{dF_{ts}}{dz} = 2E_{eff}a \quad (10)$$

where a is the contact radius and E_{eff} is the flexibility (effective elastic modulus).

Table 1: Cantilever properties (adapted from refs. 26, 32 and 45)

Eigenmode (flexural)	κ_n	Frequency	Force constant	Quality factor (no internal damping)	Optical sensitivity
n		$\omega_n = \left(\frac{\kappa_n}{\kappa_1}\right)^2 \omega_1$	$k_n = \left(\frac{\omega_n}{\omega_1}\right)^2 k_1$	$Q_n = \frac{\omega_n}{\omega_1} Q_1$	$\sigma_n = \frac{\varphi_n'}{\varphi_1'} \sigma_1$
1	1.875	$\omega_1 = \omega_0$	k_1	Q_1	σ_1
2	4.694	$6.27\omega_0$	$39.31k_1$	$6.27Q_1$	$3.473\sigma_1$
3	7.855	$17.55\omega_0$	$308k_1$	$17.55\ Q_1$	$5.706\sigma_1$
4	10.996	$34.39\omega_0$	$1183\ k_1$	$34.39\ Q_1$	$7.985\sigma_1$

References

1. Binnig, G., Quate, C. F. & Gerber, C. Atomic force microscope. *Phys. Rev. Lett.* **56,** 930-933 (1986).
2. Meyer, G. & Amer, N. M. Novel optical approach to atomic force microscopy. *Appl. Phys. Lett.* **53,** 1045-1047 (1988).
3. Garcia, R. & Perez, R. Dynamic atomic force microscopy methods. *Surf. Sci. Rep.* **47,** 197-301 (2002).
4. Giessibl, F.J. Advances in atomic force microscopy. *Rev. Mod. Phys.* **75,** 949-983 (2003).
5. Parot, P. *et al.* Past, present and future of atomic force microscopy in life sciences and medicine, *J. Mol. Recognit.* **20,** 418-431 (2007).
6. Garcia, R., Magerle, R. & Perez, R. Nanoscale compositional mapping with gentle forces. *Nature Mater.* **6,** 405-411 (2007).
7. Ando, T., Uchihashi, T. & Fukuma, T. High-speed atomic force microscopy for nano-visualization of dynamic biomolecular processes. *Prog. Surf. Sci.* **83,** 337-437 (2008).
8. Gan, Y. Atomic and subnanometer resolution in ambient conditions by atomic force microscopy. *Surf. Sci. Rep.* **64,** 99–121 (2009).
9. Klinov, D. & Magonov, S. True molecular resolution in tapping-mode atomic force microscopy with high-resolution probes. *Appl. Phys. Lett.* **84,** 2697-2699 (2004).
10. Fukuma, T., Kobayashi, K., Matsushige, K. & Yamada, H. True atomic resolution in liquid by frequency-modulation atomic force microscopy. *Appl. Phys. Lett.* **87,** 034101-3 (2005).
11. Yamada, H. *et al.* Molecular resolution imaging of protein molecules in liquid using frequency modulation atomic force microscopy. *Appl. Phys. Lett.* **2,** 095007-3 (2009).
12. Higgings, M. J., Sader, J. E. & Jarvis, S. P. Frequency modulation atomic force microscopy reveals individual intermediates with each unfolded I27 titin domain. *Biophys. J.* **90,** 640-647 (2006).
13. Kuna, J. J. *et al.* The effect of nanometre-scale structure on interfacial energy. *Nature Mater.* **8**, 837-842 (2009).
14. Baykara, M. Z., Schwendemann, T. C., Altman, E. I., & Schwarz, U. D. Three-dimensional atomic force microscopy-Taking surface imaging to the next level. *Adv. Mater.* **22,** 2838–2853 (2010).
15. Palermo, V., Palma, M. & Samori, P. Electronic characterization of organic thin films by Kelvin probe force microscopy. *Adv. Mater.* **18**, 145–164 (2006).
16. Schwarz, A. & Wiesendanger, W. Magnetic sensitive force microscopy. *Nano Today* **3,** 28–39 (2008).
17. Luan, B. & Robbins, M. O. Contact of single asperities with varying adhesion: comparing continuum mechanics to atomistic simulations. *Phys. Rev. E* **74**, 026111-17 (2006).

18. Raman, A., Melcher, J. & Tung, R. Cantilever dynamics in atomic force microscopy. *Nano Today* **3,** 20-27 (2008).
19. Stark, R.W. Bistability, higher harmonics and chaos in AFM. *Mater. Today* **13,** 24–32 (2010).
20. Butt, H.J., Capella, B. & Kappl, M. Force measurements with the atomic force microscope: Technique, interpretation and applications. *Surf. Sci. Rep.* **59**, 1-152 (2005).
21. Bizarri, A.R. & Cannistraro, S. The application of atomic force spectroscopy to the study of biological complexes undergoing a biorecognition process. *Chem. Soc. Rev.* **39**, 734-749 (2010).
22. Cross, S. E., Jin, Y.-S., Rao, J. & Gimzewski. Nanomechanical analysis of cells from cancer patients. *Nature Nanotech.* **2**, 780-783 (2007).
23. Goetz, J. G. *et al.* Biomechanical remodeling of the microenvironment by stromal caveolin-1 favors tumor invasion and metastasis. *Cell* **146**, 148-163 (2011).
24. Arlett, J. L., Myers, E. B. & Roukes, M. L. Comparative advantages of mechanical biosensors. *Nature Nanotech.* **6,** 203–215 (2011).
25. Gil-Santos, E. *et al.* Nanomechanical mass sensing and stiffness spectrometry based on two-dimensional vibrations of resonant nanowires. *Nature Nanotech.* **5**, 641-645 (2010).
26. Garcia, R. *Amplitude modulation atomic force microscopy* (Wiley-VCH, Weinhein, Germany 2010).
27. Butt, H.J. & Jascke, M. Calculation of thermal noise in atomic force microscopy, *Nanotechnology* **6**, 1-7 (1995).
    The calculation of the cantilever's thermal noise by including the contributions from all the cantilever eigenmodes makes this article a key contribution in force microscopy.
28. Rabe, U., Turner, I. & Arnold, W. Analysis of the high-frequency response of atomic force microscope levers. *Appl. Phys. A-Mater* **66**, S277-S282 (1998).
29. Sader, J.E. Frequency response of cantilever beams immersed in viscous fluids with applications to the atomic force microscope*. J. Appl. Phys.* **84**, 64-76 (1998).
30. Dürig, U. Relations between interaction force and frequency shift in large-amplitude dynamic force microscopy. *Appl. Phys. Lett.* **75**, 433-435 (1999).
31. Tamayo J, Energy dissipation in tapping-mode scanning force microscopy with low quality factors. *Appl. Phys. Lett.* **75**, 3569-3571 (1999).
32. Stark, R.W. & Heckel, W.M. Fourier transformed atomic force microscopy: tapping mode atomic force microscopy beyond the Hookian approximation. *Surf. Sci.* **457**, 219-228 (2000).
33. Rodriguez, T.R. & Garcia, R. Tip motion in amplitude modulation (tapping-mode) atomic-force microscopy: Comparison between continuous and point-mass models. *Appl. Phys. Lett.* **80**, 1646-1648 (2002).

34. Rabe, U., Janser, K. & Arnold, W. Vibrations of free and surface-coupled atomic force microscope cantilevers: Theory and experiment. *Rev. Sci. Instrum.* **67**, 3281-3293 (1996).
35. Stark, R.W., Schitter, G., Stark, M., Guckenberger, R. & Stemmer, A. State-space model of freely vibrating and surface-coupled cantilever dynamics in atomic force microscopy. *Phys. Rev. B* **69**, 085412-9 (2004).
36. Schaffer, T.E. & Fuchs, H. Optimized detection of normal vibration modes of atomic force microscope cantilevers with the optical beam deflection method. *J. Appl. Phys.* **97**, 083524-8 (2005).
37. Hsu, J.C., Lee, H.L. & Chang, W.J. Flexural vibration frequency of atomic force microscope cantilevers using Timoshenko beam theory. *Nanotechnology* **18**, 285503-5 (2007).
38. Melcher, J., Hu, S. & Raman, A. Equivalent point-mass models of continuous atomic force microscope probes. *Appl. Phys. Lett.* **91**, 053101-3 (2007).
39. Cantrell, J.H. & Cantrell, S.A. Analytical model of the nonlinear dynamics of cantilever tip-sample surface interactions for various acoustic atomic force microscopies. *Phys. Rev. B* **77**, 165409-16 (2008).
40. Kokavecz, J. & Mechler, A. Spring constant of microcantilevers in fundamental and higher eigenmodes. *Phys. Rev. B* **78**, 172101-4 (2008).
41. G. Hahner. Dynamic spring constants for higher flexural modes of cantilever plates with applications to atomic force microscopy. *Ultramicroscopy* **110**, 801-806 (2010).
42. Zypman, F. Internal damping for noncontact atomic force microscopy cantilevers. *J. Vac. Sci. Technol. B* **28**, C4E24-C4E27 (2010)
43. Abbasi, M. & Mohammadi, A.K. A new model for investigating the flexural vibration of an atomic force microscope cantilever. *Ultramicroscopy* **110**, 1374-1379 (2010).
44. Pishkenari, H. N. & Meghdari, A. Effects of higher oscillation modes on TM-AFM measurements. *Ultramicroscopy* **111**, 107-116 (2011).
45. Kiracofe, D. & Raman, A. On eigenmodes, stiffness, and sensitivity of atomic force microscope cantilevers in air versus liquids. *J. Appl. Phys.* **107**, 033506-9 (2009).
Theory and experimental study of the influence of the tip mass on the sensitivity and stiffness of the cantilever eigenmodes.

46. Dürig, U. Interaction sensing in dynamic force microscopy. *New J. Phys.* **2**, 5.1-5.12 (2000).
47. Hembacher, S., Giessibl, F. J. & Mannhart, J. Force microscopy with light-atom probes. *Science* **305,** 380–383 (2004).
First experimental result reporting of the use of higher harmonics to enhance spatial resolution in force microscopy.

48. Wright, C.A. & Solares, S.D. On mapping subangstrom electron clouds with force microscopy. *Nano Lett.* **11,** 5026-5033 (2011).

49. Xu, X., Melcher, J., Basak, S., Reinferberger, R. & Raman, A. Compositional contrast of biological materials in liquids using the momentary excitation of higher eigenmodes in dynamic AFM. *Phys. Rev. Lett.* **102**, 060801-4 (2009).
50. Stark, M., Stark, R.W., Heckl, W. H. & Guckenberger, R. Inverting dynamic force microscopy: From signals to time-resolved interaction forces. *Proc. Natl Acad. Sci. USA* **99**, 8473-8478 (2002).
Method to obtain time-resolved forces by recording the frequency spectra (higher harmonics) of the tip motion.

51. Sahin et al. High-resolution imaging of elastic properties using harmonic cantilevers. *Sen Act. A* **114**, 183-190 (2004).
52. Sarioglu, A.F. & Solgaard, O. Modeling, design, and analysis of interferometric cantilevers for time-resolved force measurements in tapping-mode atomic force microscopy. *J. Appl. Phys.* **109**, 064316-11 (2011).
53. Parlak, Z. & Degertekin, F.L. Combined quantitative ultrasonic and time-resolved interaction force AFM imaging. *Rev. Sci. Instrum.* **82**, 013703-4 (2011).
54. Sahin, O., Quate, C.F., Solgaard, O. & Atalar, A. An atomic force microscope tip designed to measure time-varying nanomechanical forces. *Nature Nanotech.* **2**, 507–514 (2007).
Measurement of time-resolved forces by using the higher harmonics of the torsional cantilever deflection. Torsional higher harmonics are easier to measure then those in the flexural deflection.
55. Rodriguez, T.R. & Garcia, R. Compositional mapping of surfaces in atomic force microscopy by excitation of the second normal mode of the cantilever. *Appl. Phys. Lett.* **84**, 449-451 (2004).
Numerical simulation-based study to enhance the force sensitivity in AFM by the simultaneous excitation of two eigenmodes. These simulations provided the framework for development of bimodal AFM.

56. Martinez, N.F. et al. Bimodal atomic force microscopy imaging of isolated antibodies in air and liquid. *Nanotechnology* **19**, 384011 (8pp) (2008).
57. Proksch, R. Multifrequency, repulsive-mode amplitude-modulated atomic force microscopy, *Appl. Phys. Lett.* **89**, 113121-3 (2006).
58. Kawai, S. et al. Systematic achievement of improved atomic-scale contrast via bimodal dynamic force microscopy. *Phys. Rev. Lett.* **103**, 220801-4 (2009).
59. Aksoy, M.D. & Atalar, A. Force spectroscopy using bimodal frequency modulation atomic force microscopy. *Phys. Rev. B* **83**, 075416-6 (2011).
60. Lozano, J.R. & R. Garcia. Theory of multifrequency AFM. *Phys. Rev. Lett.* **100,** 076102-4 (2008).
61. Martinez-Martin, D., Herruzo, E. T., Dietz, C., Gomez-Herrero J. & Garcia, R. Noninvasive protein structural fexibility mapping by bimodal dynamic force microscopy. *Phys. Rev. Lett.* **106**, 198101-4 (2011).

62. Solares, S.D. & Chawla, G. Frequency response of higher cantilever eigenmodes in bimodal and trimodal tapping mode atomic force microscopy. *Meas. Sci. Technol.* **21**, 125502 (12pp) (2010).
63. Platz, D., Tholén, E. A. & Haviland, D.B. Intermodulation atomic force microscopy. *Appl. Phys. Lett.* **92**, 153106-3 (2008).
64. Hutter, C., Platz, D., Tholen, E.A., Hansson, T.H. & Haviland, D.B. Reconstructing nonlinearities with intermodulation spectroscopy. *Phys. Rev. Lett.* **104**, 05801-4 (2010).
65. Jesse, S., Kalinin, S. V., Proksch, R., Baddorf, A.P. & Rodriguez, B.J. Energy dissipation measurements on the nanoscale: band excitation method in scanning probe microscopy. *Nanotechnology* **18**, 435503 (8pp) (2007).
66. Agarwal, P. & Salapaka, M.V. Real time estimation of equivalent cantilever parameters in tapping mode atomic force microscopy. *Appl. Phys. Lett.* **95**, 083113-3 (2009).
67. Thota, P., MacLaren, S. & Dankowitz, H. Controlling bistability in tapping mode atomic force microscopy using dual-frequency excitation. *Appl. Phys. Lett.* **91**, 093108-3 (2007).
68. Dick, A.J. & Solares, S.D. Utilizing Off-Resonance and Dual-Frequency Excitation to Distinguish Attractive and Repulsive Surface Forces in Atomic Force Microscopy. *J. Comp. Nonlin Dyn.* **6**, 031005 (12 pages) (2011).
69. Kawai, S., Kitamura, S., Kobayashi, D., Meguro, S. & Kawakatsu, H. An ultrasmall amplitude operation of dynamic force microscopy with second flexural mode. *Appl. Phys. Lett.* **86**, 193107-3 (2005).
70. Killgore, J.P., Kelly, J. Y., Stafford, C. M., Fasolka, M. J. & Hurley, D. C. Quantitative subsurface contact resonance force microscopy of model polymer nanocomposites. *Nanotechnology* **22**, 175706 (7pp) (2011).
71. Pfeiffer, O. et al. Using higher flexural modes in non-contact force microscopy. *Appl. Surf. Sci.* **157**, 337-342 (2000).
72. Dietz, C., Herruzo, E. T. , Lozano, J. R. & Garcia, R. Nanomechanical coupling enables detection and imaging of 5 nm superparamagnetic particles in liquid. *Nanotechnology* **22**, 125708 (8pp) (2011).
73. Stark, M., Stark, R.W., Heckl, W.M. & Guckenberger, R. Spectroscopy of the anharmonic cantilever oscillations in tapping-mode atomic-force microscopy. *Appl. Phys. Lett.* **77**, 3293-3295 (2000).
74. Sahin, O., Quate, C.F., Solgaard, O. & Atalar, A. Resonant harmonic response in tapping-mode atomic force microscopy. *Phys. Rev. B* **69**, 165416-9 (2004).
75. Crittenden, S., Raman, A. & Reifenberger, R. Probing attractive forces at the nanoscale using higher-harmonic dynamic force microscopy. *Phys. Rev. B* **72**, 235422-13 (2005).
76. Balantekin, M. & Atalar, A. Enhancing higher harmonics of a tapping cantilever by excitation at a submultiple of its resonance frequency. *Phys. Rev. B*. **71**, 125416-5 (2005).

77. Legleiter, J., Park, M., Cusick, B. & Kowalewski, T. Scanning probe acceleration microscopy (SPAM) in fluids: Mapping mechanical properties of surfaces at the nanoscale. *Proc. Natl Acad. Sci. USA* **103**, 4813–4818 (2006).
78. Preiner, J., Tang, J., Pastushenko, V. & Hinterdorfer, P. Higher harmonic atomic force microscopy: Imaging of biological membranes in liquid. *Phys. Rev. Lett.* **99**, 046102-4 (2007).
79. Turner, R.D., Kirkham, J., Devine, D. & Thomson, N. H. Second harmonic atomic force microscopy of living Staphylococcus aureus bacteria. *Appl. Phys. Lett.* **94**, 043901-3 (2009).
80. Raman, A. *et al.* Mapping nanomechanical properties of live cells using multiharmonic atomic force microscopy. *Nature Nanotech.* **6**, 809-813 (2011).
81. Martinez, N.F., Patil, S., Lozano, J.R. & Garcia, R. Enhanced compositional sensitivity in atomic force microscopy by the excitation of the first two flexural modes. *Appl. Phys. Lett.* **89**, 153115-3 (2006).
82. Patil, S., Martinez, N.F., Lozano, J.R. & Garcia, R. Force microscopy imaging of individual protein molecules with sub-pico Newton force sensitivity. *J. Mol. Recognit.* **20**, 516-523 (2007).
83. Dietz, C. et al. Nanotomography with enhanced resolution using bimodal atomic force microscopy. *Appl. Phys. Lett.* **92**, 143107-3 (2008).
84. Stark, R.W. Dynamics of repulsive dual-frequency atomic force microscopy, *Appl. Phys. Lett.* **94**, 063109-3 (2009).
85. Albonetti, C., Casalini, S., Borgatti, F., Floreano, L. & Biscarini, F. Morphological and mechanical properties of alkanethiol SAM investigated by bimodal AFM. *Chem. Comm.* **47**, 8823-8825 (2011).
86. Li, W., Cleveland, J.P. & Proksch, R. Bimodal magnetic force microscopy: Separation of short and long range forces. *Appl. Phys. Lett.* **94**, 163118-3 (2009).
87. Stark, R.W., Naujoks, N. & Stemmer, A. Multifrequency electrostatic force microscopy in the repulsive regime. *Nanotechnology* **18**, 065502 (7pp) (2007).
88. Bostanci, U., Abak, M. K., Aktas, O. & Dâna, A. Nanoscale charging hysteresis measurements by multifrequency electrostatic force spectroscopy. *Appl. Phys. Lett.* **92**, 093108-3 (2008).
89. Kawai, S. *et al.* Ultrasensitive detection of lateral atomic-scale interactions on graphite (0001) via bimodal dynamic force measurements. *Phys. Rev. B* **81**, 085420-7 (2010).
Bimodal excitation and detection of flexural and torsional modes compatible with frequency modulation AFM and ultra high vacuum environments.

90. Balke, N. *et al.* Nanoscale mapping of ion diffusion in a lithium-ion battery cathode. *Nature Nanotech.* **5**, 749–754 (2010).
The multiparameter acquisition capabilities of the band excitation method is exploited to generate nanscale maps of Li-ion migration in batteries.

91. Balke, N. *et al.* Real space mapping of Li-Ion transport in amorphous Si anodes with nanometer resolution*. Nano Lett.* **10**, 3420–3425 (2010).
92. Sahin, O., Erina, N. High-resolution and large dynamic range nanomechanical mapping in tapping-mode atomic force microscopy. *Nanotechnology* **19**, 445717 (9pp) (2008).
93. Dong, M., Husale, S. & Sahin, O. Determination of protein structural flexibility by microsecond force spectroscopy. *Nature Nanotech.* **4**, 514–517 (2009).
94. Husale, S., Persson, H.H.J. & O. Sahin. DNA nanomechanics allows direct digital detection of complementary DNA and microRNA targets. *Nature* **462**, 1075-1078 (2009).
95. Dong, M. & Sahin, O. A nanomechanical interface to rapid single-molecule interactions. *Nature Commun*. **2**, 247 (2011).
96. Dokukin, M.E., Guz, N.V., Gaikwad, R.M., Woodworth, C.D. & Sokolov, I., Cell surface as a fractal: Normal and cancerous cervical cells demonstrate different fractal behavior of surface adhesion maps at the nanoscale. *Phys. Rev. Lett.* **107**, 028101-4 (2011).
97. Kolosov, O. & Yamanaka, K. Nonlinear detection of ultrasonic vibrations in an atomic-force microscope. *Jpn. J. Appl. Phys.* **32**, L1095-L1098 (1993).
98. Hu, S., Su, C. & Arnold, W. J. Imaging of subsurface structures using atomic force acoustic microscopy at GHz frequencies. *J. Appl. Phys.* **109**, 084324-5 (2011).
99. Shekhawat, G. S. & Dravid, V. P. Nanoscale imaging of buried structures via scanning near-field ultrasound holography. *Science* **310**, 89–92 (2005).
First contribution reporting nanomechanical holography experiments. Images showing subsurface features in microelectronic devices and cells are reported.
100. Tetard, L., Passian, A. & Thundat, T. New modes for subsurface atomic force microscopy through nanomechanical coupling. *Nature Nanotech.* **5**, 105–109 (2010).
101. Tetard, L. *et al.* Elastic phase response of silica nanoparticles buried in soft matter. *Appl. Phys. Lett.* **93**, 133113-3 (2008).
102. Tetard, L. *et al.* Imaging nanoparticles in cells by nanomechanical holography. *Nature Nanotech.* **3**, 501–505 (2008).
103. Shekhawat, G., Srivastava, A., Avashty, S. & Dravid, V. Ultrasound holography for noninvasive imaging of buried defects and interfaces for advanced interconnect architectures. *Appl. Phys. Lett.* **95**, 263101-3 (2009).
104. Garcia-Sanchez, D., Paulo, A.S., Esplandiu, M.J., Perez-Murano, F. & Bachtold, A. Mechanical detection of carbon nanotube resonator vibrations. *Phys. Rev. Lett.* **99**, 085501-4 (2007).
105. Garcia-Sanchez, D. *et al.* Imaging mechanical vibrations in suspended graphene sheets. *Nano Lett.* **8,** 1399-1403 (2008).
106. Garcia, R. Probe microscopy: Images from below the surface. *Nature Nanotech.* **5,** 101–102 (2010).

107. Diebold, A. C. Subsurface Imaging with Scanning Ultrasound Holography. *Science* **310,** 61–62 (2005).

Figure 1. Microcantilever dynamics in force microscopy. **a**, Scanning electron microscope image of a Si cantilever. **b**, Modal shapes of the first three flexural eigenmodes of a rectangular (tipless) cantilever that is clamped at one end and free at the other end. **c**, Amplitude response as a function of the excitation frequency for a rectangular cantilever (simulation). **d**, Scheme of the interaction between a vibrating cantilever and a nonlinear tip-surface force. **e**, Frequency response of a rectangular cantilever under the influence of a nonlinear force (simulation). An enhancement of the amplitudes of the 6^{th} and 17^{th} harmonics is observed due to the coupling, respectively, with the 2^{nd} and 3^{rd} eigenmodes. **f**, Higher harmonic image of a tungsten tip imaging a graphite surface (ref. 47). The four-leaved clover is related to the 4 fold symmetry of charge density maxima in an W adatom on W(100).

Figure 2. Multifrequency AFM evolution and approaches. **a,** Some milestones in the evolution of multifrequency AFM. **b**, Bimodal AFM scheme. The amplitude of the 1^{st} mode is used for topography imaging while the signal from the 2^{nd} mode give access to different mechanical or electromagnetic properties (adapted from 56). **c**, Scheme of the band excitation method. The excitation signal is digitally synthesized to have a predefined amplitude and phase in a given frequency window. The cantilever response is detected and Fourier transformed at each pixel in an image (adapted from ref. 65). **d**, Scanning electron microscopy image of a torsional harmonics cantilever and scheme (adapted from ref. 54). The force is obtained from the higher harmonics components in the torsional signal. **e**, Scheme of a nanomechanical holography set-up. The probe and the sample are mechanically excited by signals that contain a number of known frequency components. From these frequency components, the tip-sample interaction synthesizes new modes (*S* signal) which carry information on the subsurface structures (adapted from ref. 106).

Figure 3. Topography and flexibility mapping of proteins. a, Flexibility map of a purple membrane sheet showing extracellular (EC) and cytoplasmatic (CP) sides. **b**, The cross-section shows the variations along the line marked in Fig. 3a. **c**, High-resolution flexibility image of a region of the EC side. The image shows the protein trimers arranged in a lattice with a parameter of 6 nm. The contrast arises from changes in the elasticity between the proteins and the lipids regions (**a**-**c**, adapted from ref. 93). **d,** Bimodal AFM topography. **e**, Flexibility map of a single IgM antibody taken simultaneously with (d). The image has been obtained by applying very small forces (40 pN). **f**, Flexibility profile along the line marked in Fig. 3d. The profile shows local variations of the flexibility that are consistent with the orientation flexibility of the antibody complex when its binds a cell surface antigen are unrelated to major topographic features (**d**-**f**, adapted from ref. 61).

Figure 4. Mapping high frequency oscillations, ion diffusion and subsurface structures. a, Scheme to image the spatial shape of vibrations in nanoscale resonators. A signal modulated at the frequency of the cantilever 1^{st} eigenmode is used to excite the resonator. **b**, Spatial shape of the first three modes of a carbon nanotube

suspended between two gold electrodes (adapted from ref. 104). **c**, Scheme of the band excitation experiment to measure ion diffusion in a battery. Lipon is the electrolyte. It stands for lithium phosphorus oxynitrided. **d**, AFM deflection image of some grain interfaces in the electrode. **e**, Images of the regions that concentrate the Li-ions (in red) during battery charging (**c**-**e**, adapted from ref. 91). **f**, Cross-section of a cell. **g**, Nanomechanical holography image of a mouse cell. **h**, Conventional AFM image of the same cell (adapted from refs. 99, 107).

Figure 1

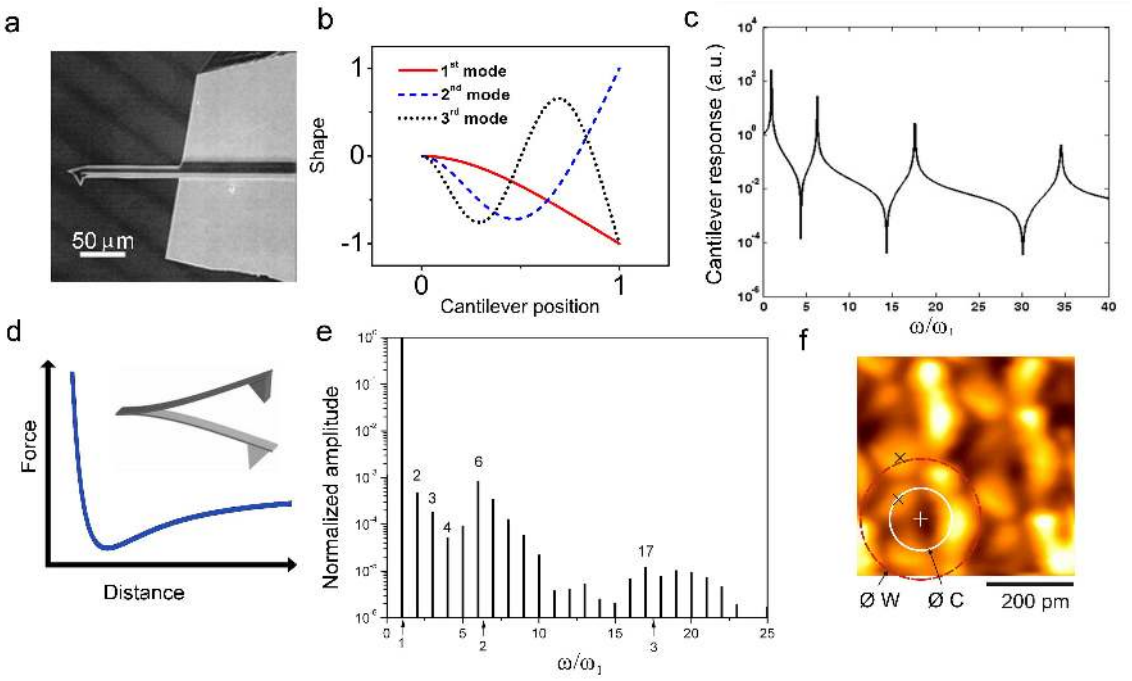
a
50 µm
b
1st mode
2nd mode
3rd mode
Shape
Cantilever position
c
Cantilever response (a.u.)
ω/ω1
d
Force
Distance
e
Normalized amplitude
2
3
4
6
17
ω/ω1
f
Ø W
Ø C
200 pm

Figure 2

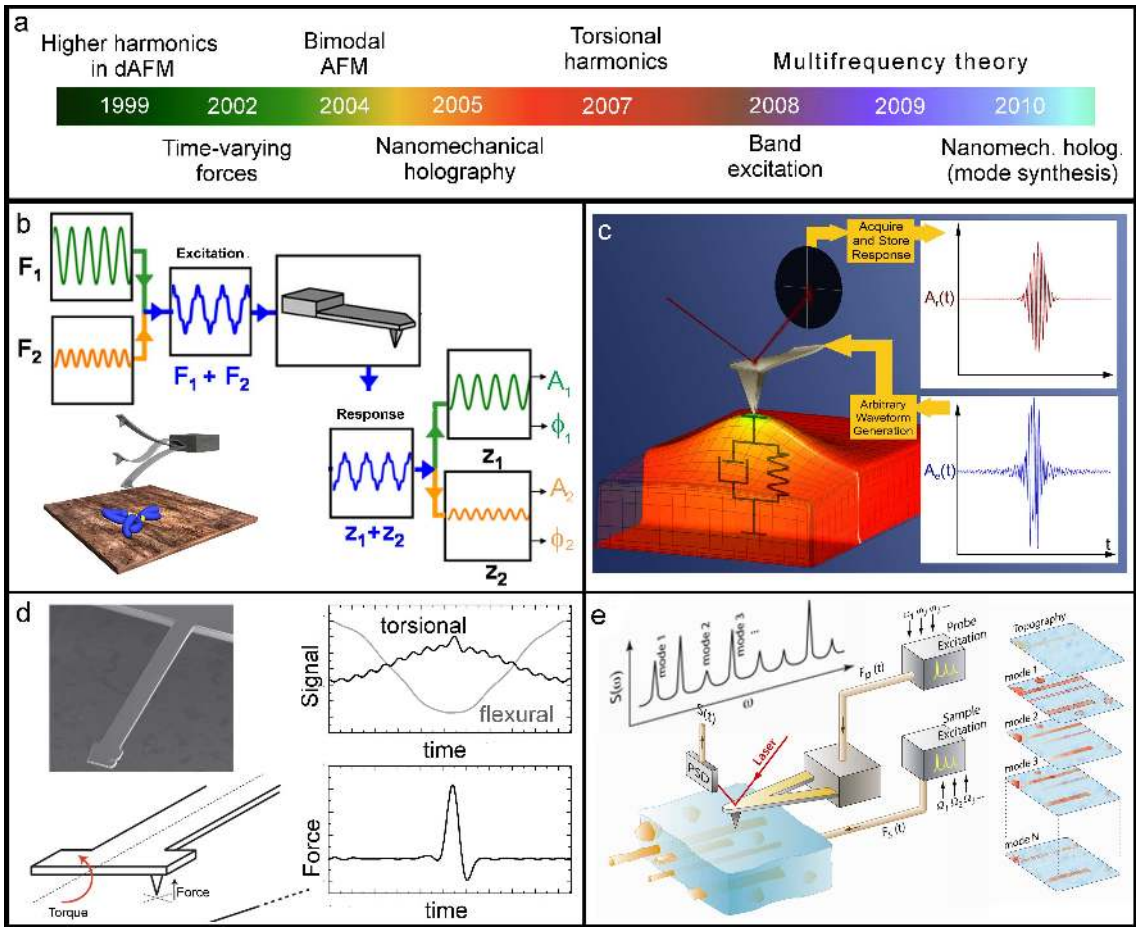
a
Higher harmonics in dAFM
Bimodal AFM
Torsional harmonics
Multifrequency theory
1999
2002
2004
2005
2007
2008
2009
2010
Time-varying forces
Nanomechanical holography
Band excitation
Nanomech. holog. (mode synthesis)
b
F1
F2
Excitation
F1 + F2
Response
z1+z2
A1
ϕ1
z1
A2
ϕ2
z2
c
Acquire and Store Response
Arbitrary Waveform Generation
d
torsional
flexural
Signal
time
Force
time
Torque
Force
e
mode 1
mode 2
mode 3
Probe Excitation
Sample Excitation
Laser
PSD
Topography
mode 1
mode 2
mode 3
mode N

Figure 3

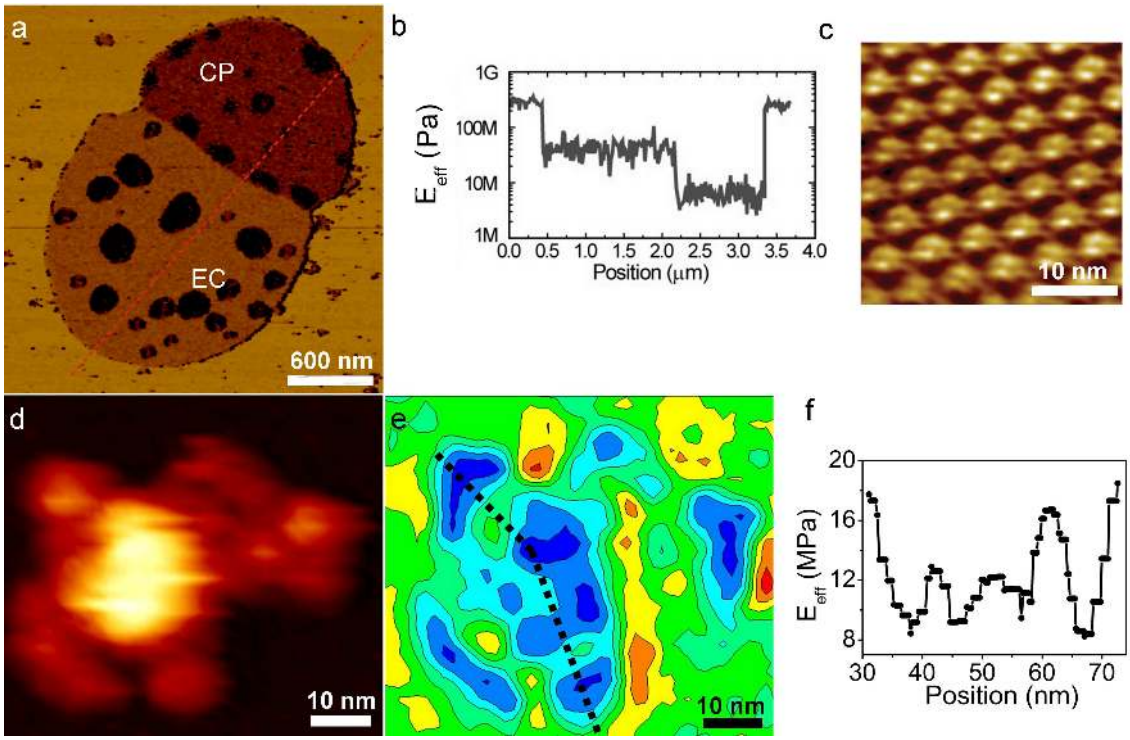
a
CP
EC
600 nm
b
1G
100M
10M
1M
E_{eff} (Pa)
0.0 0.5 1.0 1.5 2.0 2.5 3.0 3.5 4.0
Position (μm)
c
10 nm
d
10 nm
e
10 nm
f
20
16
12
8
E_{eff} (MPa)
30 40 50 60 70
Position (nm)

Figure 4

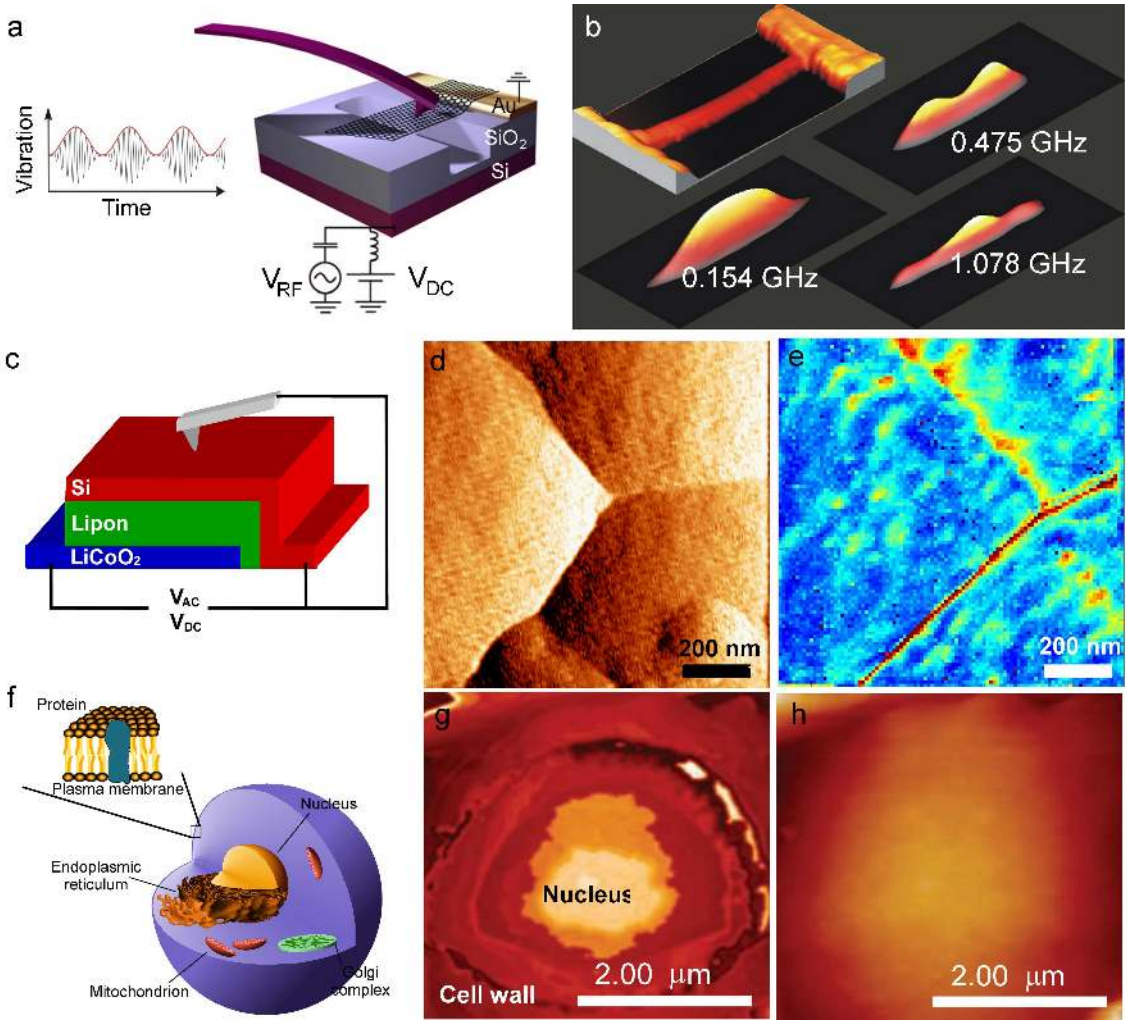
a
Vibration
Time
Au
SiO_2
Si
V_{RF}
V_{DC}
b
0.475 GHz
0.154 GHz
1.078 GHz
c
Si
Lipon
$LiCoO_2$
V_{AC}
V_{DC}
d
200 nm
e
200 nm
f
Protein
Plasma membrane
Nucleus
Endoplasmic reticulum
Mitochondrion
Golgi complex
g
Nucleus
Cell wall
2.00 μm
h
2.00 μm